ACS OMEGA

Open Access

http://pubs.acs.org/journal/acsodf

Article

Comparative Study of Enzymatic Lipolysis Using Nanofructosome-Coated CalB Lipase Encapsulated in Silica and Immobilized on Silica-Coated Magnetic Nanoparticles

Woo Young Jang,[‖] Yu Jeong Kim,[‖] and Jeong Ho Chang*

Cite This: *ACS Omega* 2025, 10, 13319−13326

Read Online

ACCESS | Metrics & More | Article Recommendations

ABSTRACT: This study evaluates the enzymatic lipolysis performance of nanofructosome-coated CalB lipase (CalB@NF) encapsulated in silica and immobilized on silica-coated magnetic nanoparticles (Si-MNP) for converting natural olive oil to oleic acid. The nanofructosome coating, composed of levan, a nanosized fructan polymer, was applied to enhance the heat and acid resistance of the CalB enzyme. To further improve functionality, CalB@NF was encapsulated in silica (CalB@NF@SiO_2) or immobilized on Si-MNP using a chloropropylsilane linker. The silica-encapsulated CalB@NF (CalB@NF@SiO_2) was synthesized via a sol−gel process, resulting in an average particle size of 304 nm, while the immobilized CalB@NF on Si-MNP exhibited a smaller average particle size of 58 nm. Quantitative determination of CalB in both formulations was conducted using the Bradford assay, yielding concentrations of 19.5 μg/mL for CalB@NF@SiO_2 and 44.9 μg/mL for CalB@NF@Si-MNP. Enzymatic lipolysis was evaluated by measuring the production of oleic acid from natural olive oil. CalB@NF@Si-MNP achieved complete lipolysis within 3 h, whereas CalB@NF@SiO_2 required 24 h to reach the same result. The lipolysis rates were 0.92 mmol/h for CalB@NF@Si-MNP and 0.21 mmol/h for CalB@NF@SiO_2, indicating that CalB@NF@Si-MNP was 4.5 times faster. Regarding reusability, CalB@NF@SiO_2 retained 20% more activity compared to CalB@NF@Si-MNP. While the reusability of CalB@NF@Si-MNP decreased to 76% after the first cycle, CalB@NF@SiO_2 maintained nearly 100% reusability across multiple cycles. These results highlight the complementary strengths of the two formulations: CalB@NF@SiO_2 offers controlled lipolysis rates, high stability, and excellent reusability, whereas CalB@NF@Si-MNP excels in rapid lipolysis. Both silica encapsulation and silica-coated magnetic nanoparticles demonstrate substantial potential for optimizing enzyme activity, stability, and reusability in diverse applications.

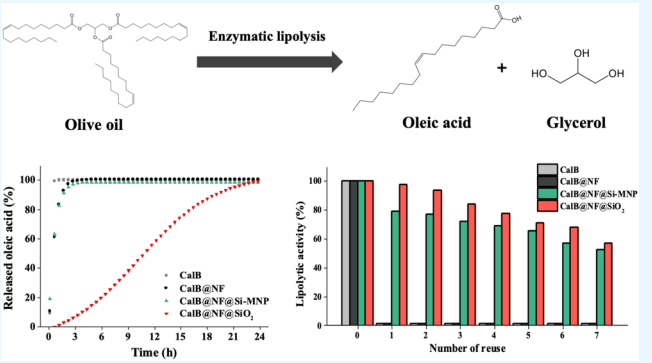

1. INTRODUCTION

Lipase enzymes are extensively utilized across various industries, including food processing,[1,2] chemical manufacturing,[3−7] and biodiesel production,[8−10] due to their capability to catalyze lipid hydrolysis and esterification reactions. The growing emphasis on sustainable industrial practices has propelled lipases into the spotlight as key enablers of green chemistry. Recent studies have demonstrated that lipase-mediated processes can significantly reduce energy consumption and waste generation, thereby offering environmentally friendly alternatives in the synthesis of high-value chemicals and biofuels.[11−17] Moreover, the inherent catalytic efficiency and selectivity of lipases have led to innovations in process design, making them attractive candidates for eco-friendly manufacturing and biocatalytic transformations. This evolving landscape highlights the need for advanced enzyme immobilization strategies that not only enhance stability and reusability but also facilitate integration into diverse industrial processes. Among these, *Candida antarctica* lipase B (CalB) has emerged as a critical enzyme in numerous industrial applications, owing to its unique features such as broad substrate specificity, optimal activity at neutral pH, compatibility with nonaqueous environments, and structural flexibility under specific conditions.[18] Despite these advantages, CalB faces significant challenges, including high production costs, low resistance to organic solvents, and sensitivity to temperature fluctuations, all of which hinder its long-term stability.[19]

To address these limitations, Novozyme 435, a formulation of CalB immobilized on an acrylic resin, was developed and

Received: December 12, 2024
Revised: January 14, 2025
Accepted: March 20, 2025
Published: March 26, 2025

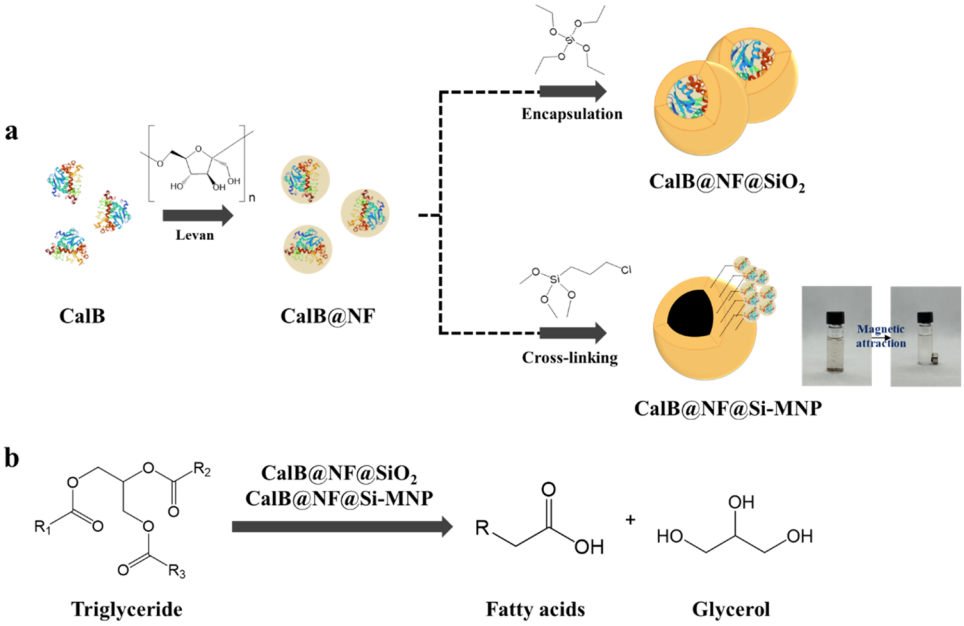

Figure 1. (a) Schematic representation of CalB@NF encapsulation in silica and immobilization on Si-MNP via cross-linking through chlorosilane modification and (b) enzymatic lipolysis process from triglyceride to fatty acid.

has gained widespread adoption in industrial applications.[20,21] While effective, Novozyme 435 also has certain drawbacks, including high costs, enzyme leaching in specific media, and solubility issues in organic solvents. Furthermore, enzymes immobilized on acrylic supports often necessitate additional separation steps, such as centrifugation and filtration, which increase the process time and complexity. These limitations underscore the need for alternative immobilization techniques to enhance the performance and cost-efficiency of CalB in industrial processes.[22,23]

Levan has emerged as a promising support material to address these challenges. As a water-soluble fructan composed of β-2,6 glycosidic linkages, levan is an environmentally friendly natural polysaccharide.[24,25] Its amphiphilic nature, attributed to its carboxyl and hydroxyl groups, enables it to form highly stable globular conformations in aqueous solutions under specific conditions. These properties make levan an excellent candidate for preparing nanofructosomes encapsulating enzymes like CalB. CalB immobilized on levan (CalB@NF) has demonstrated significant potential in reducing enzymatic activity loss under various conditions while maintaining high activity during long-term processes.[26,27] Studies have shown that CalB@NF exhibits up to a 10% increase in stability under extreme pH conditions and up to a 20% increase in stability at high temperatures compared to CalB.[28,29] However, while water-soluble supports, such as levan, provide notable benefits, they do not adequately address the high cost of CalB, highlighting the need for strategies to enhance its reusability.

Notable support materials for enhancing enzyme reusability include silica,[28−31] and magnetic particles.[32−34] Silica enables complete enzyme encapsulation through the sol−gel process, shielding enzymes from environmental stressors and providing robust physical stability, such as resistance to heat and acids. Additionally, the hydroxyl groups (−OH) on silica surfaces enhance cross-linking, stabilizing encapsulated enzymes and enabling further functionalization.[35−37] In contrast, magnetic particles facilitate efficient enzyme recovery due to their magnetic properties, significantly reducing separation time.[38−40] However, their susceptibility to rust and corrosion under fluctuating environmental conditions necessitates a silica coating to improve their stability. Silica-based immobilization techniques thus allow for two primary approaches: the full encapsulation of CalB@NF or its immobilization on silica-coated magnetic nanoparticles. These methods provide flexibility for tailoring enzyme immobilization to specific industrial process requirements.

In this study, the enzymatic lipolysis of CalB@NF encapsulated in silica (CalB@NF@SiO_2) was compared to that of CalB@NF immobilized on silica-coated magnetic nanoparticles (CalB@NF@Si-MNP) to evaluate the conversion efficiency of olive oil to oleic acid (Figure 1a). We focused on how these two immobilization strategies influence catalytic activity, enzyme loading, and reusability under real-world conditions, given the industrial significance of lipase-based technologies. A natural olive oil substrate with high oleic acid content was selected to assess the effectiveness of each formulation in generating valuable fatty acids (Figure 1b), with verification via ^{1}H NMR spectroscopy. By systematically comparing these two immobilization methods, we not only highlight the role of silica encapsulation and magnetic-nanoparticle-based immobilization in stabilizing CalB but also provide insights into designing enzyme formulations with the potential for repeated, cost-effective use in various applications.

2. EXPERIMENTAL SECTION

2.1. Materials. *C. antarctica* lipase B (CalB) and nanofructosome-coated *C. antarctica* lipase B (CalB@NF, 33 kDa) were obtained from the Korea Research Institute of Bioscience and Biotechnology (Korea) and used in encapsulation and immobilization. Oleic acid, poly(oxyethylene nonylphenylether) (Igepal CO-520), tetraethyl orthosilicate (TEOS), ferric chloride hexahydrate ($FeCl_3{\cdot}6H_2O$), ferrous chloride tetrahydrate ($FeCl_2{\cdot}4H_2O$), bovine serum albumin, tris base, phosphate buffer saline (PBS), Coomassie brilliant blue G-250

https://doi.org/10.1021/acsomega.4c11216
ACS Omega 2025, 10, 13319−13326

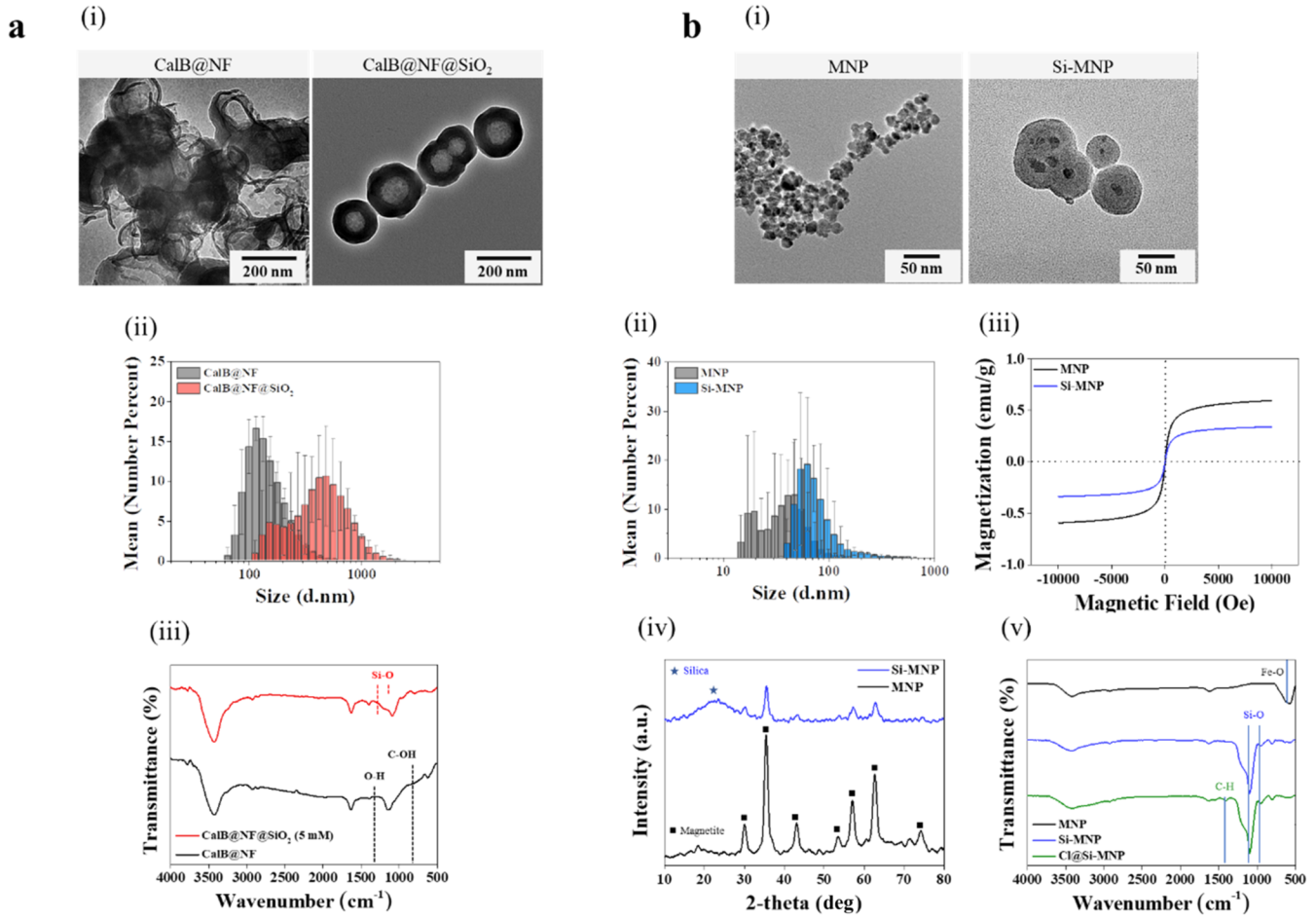

Figure 2. Characterization of (a) CalB@NF encapsulated in a silica matrix: (i) TEM images, (ii) particle size distribution, and (iii) FT-IR spectra of CalB@NF and CalB@NF@SiO_2; (b) silica-coated magnetic nanoparticles prepared for immobilization of CalB@NF: (i) TEM images, (ii) particle size distribution, (iii) magnetic susceptibility, (iv) XRD pattern, and (v) FT-IR spectra of MNP and Si-MNP.

(U.K), phosphoric acid, benzoic anhydride, and benzyl alcohol were purchased from Sigma-Aldrich. 3-chloropropyltriethoxysilane (CPTES) was purchased from Gelest. Cyclohexane, toluene, ammonia solution (28:30%), ethanol (99%), methanol, glacial acetic acid, and *n*-hexane were purchased from Daejung (Korea).

2.2. Preparation of Silica-Encapsulated CalB@NF (CalB@NF@SiO_2). CalB@NF@SiO_2 were prepared by sol−gel method, as reported in our previous work.[30] 2 mL of oleic acid, 24 g of Igepal CO-520, and 90 mg of CalB@NF were mixed to 420 mL of cyclohexane. 5 mM of TEOS was added and stirred for 1 h. Then, ammonia solution was added and stirred for 20 h. After the stirring is complete, methanol is added to confirm the formation of the precipitate, and the supernatant is then removed. The precipitate was washed three times with *n*-hexane and vacuum-dried for 24 h.

2.3. Preparation of Silica-Coated Magnetic Nanoparticles Immobilized CalB@NF (CalB@NF@Si-MNP). The MNP and Si-MNP for CalB@NF were prepared by the coprecipitation and sol−gel method.[41,42] In addition, CalB@NF@Si-MNP was surface-modified by chlorosilane to effectively immobilized CalB@NF (Cl@Si-MNP). The process of surface modification of Si-MNP was as follows.[32] Si-MNP (500 mg) was added to toluene (100 mL), stirred, and distilled water (0.125 g) was added dropwise. The temperature was raised to 60 °C, 3-chloropropyltriethoxysilane (0.65 g) was added dropwise, the temperature was raised to 110 °C, and the solution was refluxed for 24 h. After the reaction was completed, the Cl@Si-MNP obtained with a magnet was washed with distilled water and ethanol and dried under a vacuum. Subsequently, CalB@NF@Si-MNP was prepared using Cl@Si-MNP as follows. The prepared Cl@Si-MNP (50 mg) was dispersed in cyclohexane (20 mL), and then, CalB@NF was added to disperse it. The dispersed mixture was reacted on a roller at room temperature for 24 h. After the reaction was completed, the product CalB@NF@Si-MNP was washed with cyclohexane and vacuum-dried for 24 h.

2.4. Quantification of CalB Amounts in CalB@NF, CalB@NF@SiO_2, and CalB@NF@Si-MNP. The amount of CalB in CalB@NF, CalB@NF@SiO_2, and CalB@NF@Si-MNP was confirmed by Bradford assay.[43,44] Dissolve 50 mL of ethanol and 100 mg of Coomassie brilliant blue G-250 in a 1 L volumetric flask. Then, 100 mL of 85% (w/v) phosphoric acid is added, and distilled water is added to the final volume. The enzyme content was evaluated based on standard solutions and estimated by comparing concentration differences. BSA was used as a standard. The absorbance was measured at 595 nm by a UV−visible spectrophotometer.

2.5. Enzymatic Lipolysis and Reusability for Natural Olive Oil with CalB, CalB@NF, CalB@NF@SiO_2, and CalB@NF@Si-MNP. The enzymatic lipolysis of olive oil using CalB, CalB@NF, CalB@NF@SiO_2, and CalB@NF@Si-MNP

https://doi.org/10.1021/acsomega.4c11216
ACS Omega 2025, 10, 13319−13326

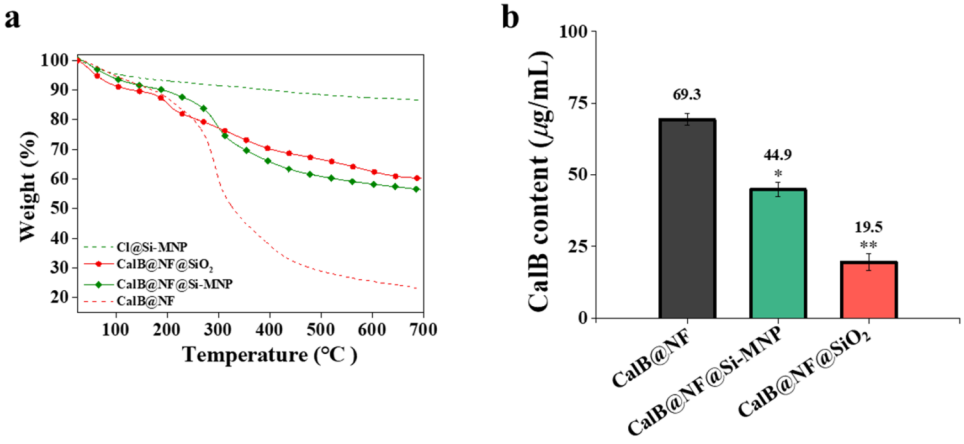

Figure 3. (a) Thermogravimetric analysis (TGA) of Cl@Si-MNP, CalB@NF@SiO_2, CalB@NF@Si-MNP, and CalB@NF, demonstrating thermal stability and weight loss associated with organic content. (b) CalB content measured using the Bradford assay, providing a quantitative comparison of enzyme loading across samples ($p < 0.05$).

was conducted as follows. 50 mM of Tris-HCl buffer (pH 8, 0.5 mL) was added to olive oil (10 mL) and stirred at 45 °C for 1 h. Subsequently, a mixed solution of Tris-HCl buffer (9.5 mL) and respective enzymes (CalB, CalB@NF, CalB@NF@SiO_2, and CalB@NF@Si-MNP) was added, and the mixture was stirred at 45 °C for an additional 24 h. After the mixture was stirred, the supernatant and precipitate were separated by centrifugation for analysis. Reusability tests were conducted by repeating the above process seven times using each isolated precipitate.

2.6. Instrumental Analysis. The morphological characteristics of CalB@NF, CalB@NF@SiO_2, MNP, and Si-MNP were evaluated by transmission electron microscope (TEM) using a JEM-2100Plus (JEOL, Tokyo, Japan) at an accelerating voltage of 200 kV. The particle sizes of CalB@NF, CalB@NF@SiO_2, MNP, and Si-MNP were measured via dynamic light scattering (DLS) using a Nano-ZS (Malvern, U.K.). Fourier transform infrared (FT-IR) spectroscopy was identified with the KBr method using Frontier (PerkinElmer) for characterization of CalB@NF, CalB@NF@SiO_2, MNP, Si-MNP, and Cl@Si-MNP. The magnetization of MNP and Si-MNP was measured using a vibrating sample magnetometer (VSM, Lake Shore, Model 7404) at room temperature (maximum of 1 T and 300 K). The phase of MNP and Si-MNP was determined through X-ray diffraction (XRD) in the 2-theta range 10−80 ° using Miniflex600 (RIGAKU, Japan). To evaluate the amount of enzyme encapsulated in CalB@NF@SiO_2 and immobilized on Cl@Si-MNP, thermogravimetric analysis (TGA) was performed using a Q600 TA Instruments (Waters) from room temperature to 700 °C (10 °C/min) in a nitrogen atmosphere. UV−visible spectrophotometry was measured by Mega 900 (SCINCO, Korea). ^{1}H NMR spectra were measured on a Bruker Advance III 400 spectrometer (400 MHz, Korea) using $CDCl_3$ solutions and tetramethylsilane as an internal standard. Chemical shifts are reported in parts per million (ppm, d) relative to the internal tetramethylsilane standard (TMS, d 0.00).

3. RESULTS AND DISCUSSION

Figure 2 shows a comparative characterization of CalB@NF, CalB@NF@SiO_2, MNP, and Si-MNP. CalB@NF was prepared by trapping CalB using levan, while MNP was synthesized via the coprecipitation method. Figure 2a shows that CalB@NF@SiO_2 was silica-coated using the sol−gel method with TEOS as the silica precursor on the surface of the CalB@NF particles. Figure 2a(i) shows the morphological details of CalB@NF and CalB@NF@SiO_2 observed through transmission electron microscopy (TEM). The morphology of CalB@NF was challenging to characterize due to its irregular structure, while CalB@NF@SiO_2 appeared spherical with a silica shell approximately 55 nm thick. This silica shell, formed by TEOS during the encapsulation process, is physically associated with CalB@NF and offers protection without forming chemical bonds. Figure 2a(ii) shows the particle size distribution of CalB@NF and CalB@NF@SiO_2. The particle sizes of CalB@NF exhibited a normal distribution with a d_{50} value of 156 nm, whereas CalB@NF@SiO_2 showed a broader distribution with a d_{50} value of 304 nm. Figure 2a(iii) displays the FT-IR spectra of CalB@NF and CalB@NF@SiO_2. Both samples exhibited a characteristic O−H stretching vibration at 3500 cm^{-1}. In CalB@NF, the C−O−C stretching vibration and aromatic C−O−C bending were observed at 1150 and 630 cm^{-1}, respectively, indicating the presence of levan. For CalB@NF@SiO_2, the asymmetric and symmetric stretching vibrations of Si−O bonds at 1080 and 970 cm^{-1} confirmed the successful encapsulation of silica.

Figure 2b shows that Si-MNP was silica-coated using the sol−gel method, with TEOS as the silica precursor applied to the surface of MNP. Figure 2b(i) presents the morphological details of the MNP and Si-MNP observed by TEM. MNP appeared as agglomerates of nanosized polygonal particles, whereas Si-MNP exhibited a spherical morphology with an average silica shell thickness of 35 nm. The silica shell, formed by TEOS, encapsulated the MNP core particles. Figure 2b(ii) shows the particle size distribution of MNP and Si-MNP. The particle sizes of both MNP and Si-MNP followed a normal distribution, with d_{50} values of 21 and 58 nm, respectively, indicating that Si-MNP were 2.5 times larger than MNP due to the silica coating. Figure 2b(iii) shows the VSM measurements of MNP and Si-MNP. The magnetic susceptibility of MNP and Si-MNP was 0.6 and 0.3 emu/g at 300 K, respectively. Despite the reduced magnetic susceptibility of Si-MNP, they could still be magnetically separated within 1 min when dispersed in water by shaking or sonication. The decrease in magnetic susceptibility for Si-MNP was attributed to the presence of the silica shell. Figure 2b(iv) shows the XRD patterns of the MNP

https://doi.org/10.1021/acsomega.4c11216
ACS Omega 2025, 10, 13319−13326

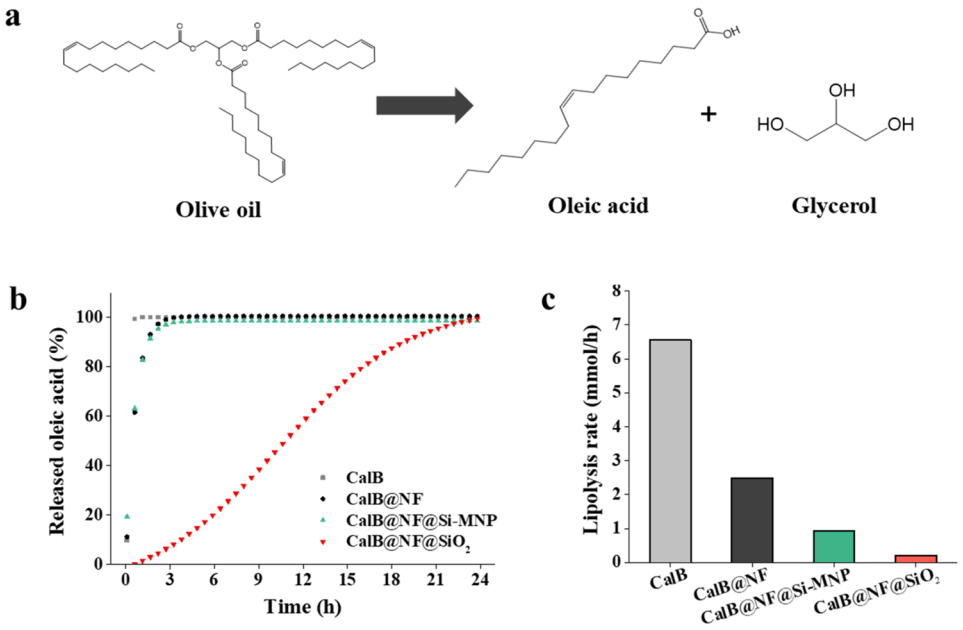

Figure 4. (a) Schematic representation of the enzymatic lipolysis process using olive oil. (b) Release of oleic acid over time during the lipolysis reaction. (c) Lipolysis rate comparison for CalB, CalB@NF, CalB@NF@Si-MNP, and CalB@NF@SiO_2, highlighting the enzymatic activity of each sample.

and Si-MNP. MNP displayed diffraction peaks at 2θ = 35.4, 57.3, and 63.2°, corresponding to the (311), (511), and (400) planes of Fe_3O_4. Si-MNP exhibited similar Fe_3O_4 peaks but with additional broad peaks at low diffraction angles (20−27°), indicating the presence of an amorphous silica shell. The intensity of the MNP peaks in the Si-MNP pattern was significantly reduced due to the silica coating. Figure 2b(v) shows the FT-IR spectra of MNP, Si-MNP, and Cl@Si-MNP. The MNP spectrum confirmed the presence of Fe−O and O−H bonds at 750 and 3400 cm^{-1}, respectively. For Si-MNP, in addition to the Fe−O and O−H peaks, Si−O bonds were observed at 1080 and 970 cm^{-1}, confirming successful silica coating. XRD and FT-IR analyses collectively verified the presence of the silica shell, confirming that the MNP core retained its intrinsic properties despite the coating. The silica coating on the MNP prevents rusting and maintains magnetism in aqueous solutions. Additionally, the abundance of −OH groups on the silica surface enhances enzyme immobilization. To further functionalize Si-MNP, the surface was treated with CPTES, resulting in Cl@Si-MNP. The FT-IR spectrum of Cl@Si-MNP confirmed the surface modification by showing characteristic C−H vibrations of CPTES at 2915 cm^{-1}. This chloro-functionalized silane layer on Si-MNP facilitates subsequent enzyme immobilization by providing reactive chloro groups that can form covalent bonds with nucleophilic residues (e.g., amino groups) on the enzyme, thereby improving the stability and attachment of CalB.

Figure 3 shows the TGA analysis and Bradford assay results of CalB@NF@SiO_2 and CalB@NF@Si-MNP. Figure 3a shows the TGA analysis of Cl@Si-MNP, CalB@NF@SiO_2, CalB@NF@Si-MNP, and CalB@NF over a temperature range of 25−700 °C, assessing weight changes associated with thermal degradation. At 700 °C, the residual weights of Cl@Si-MNP and CalB@NF@Si-MNP were 86.66% and 56.43%, respectively, indicating that 30.23% of the weight in CalB@NF@Si-MNP was due to the immobilized CalB@NF on Cl@Si-MNP. Similarly, the residual weights of CalB@NF and CalB@NF@SiO_2 were 22.95 and 60.28%, respectively, with 37.33% of the weight in CalB@NF@SiO_2 attributed to silica encapsulation. Figure 3b shows the Bradford assay results for quantifying the CalB content in CalB@NF, CalB@NF@Si-MNP, and CalB@NF@SiO_2. To ensure that the Coomassie brilliant blue G-250 could bind to the accessible portions of the enzyme, each sample at equivalent weights was thoroughly dispersed in the Bradford reagent before measurement at λ = 595 nm using UV−visible spectroscopy. Under these conditions, the measured CalB content for CalB@NF, CalB@NF@Si-MNP, and CalB@NF@SiO_2 was 69.3, 44.9, and 19.5 μg/mL, respectively. Statistical analysis showed significant differences between CalB@NF and the other two formulations, with $p < 0.05$ in both cases. The ratio of CalB immobilized to that encapsulated in silica was approximately 2:1.

Figure 4 shows the results for the lipolysis of CalB, CalB@NF, CalB@NF@Si-MNP, and CalB@NF@SiO_2. Figure 4a shows the enzymatic lipolysis process with olive oil, which consists of esterified oleic acid to a glycerol molecule. CalB lipases can break down this ester bond, releasing oleic acid and glycerol. Olive oil typically contains a complex mixture of oleic, palmitic, and linoleic acids bound to glycerol, but for this study, olive oil with up to 83% oleic acid content was used to evaluate enzymatic lipolysis. The high oleic acid content was chosen for its stability, which minimizes interference with the enzymes during the reaction. The enzyme amounts used for the decomposition were based on the CalB content quantified in Figure 4b, with samples of CalB@NF (6.7 g), CalB@NF@Si-MNP (10.4 g), and CalB@NF@SiO_2 (24.0 g) corresponding to 1.0 g of CalB. Figure 4b shows the release of oleic acid during lipolysis by CalB, CalB@NF, CalB@NF@Si-MNP, and CalB@NF@SiO_2. The oleic acid released from CalB, CalB@NF, and CalB@NF@Si-MNP increased rapidly initially and then plateaued. In contrast, CalB@NF@SiO_2 released oleic acid more slowly over 24 h. Specifically, CalB released 100% of oleic acid within 45 min, while CalB@NF and CalB@NF@Si-MNP took 2 h to reach this point. CalB@NF@Si-MNP

https://doi.org/10.1021/acsomega.4c11216
ACS Omega 2025, 10, 13319−13326

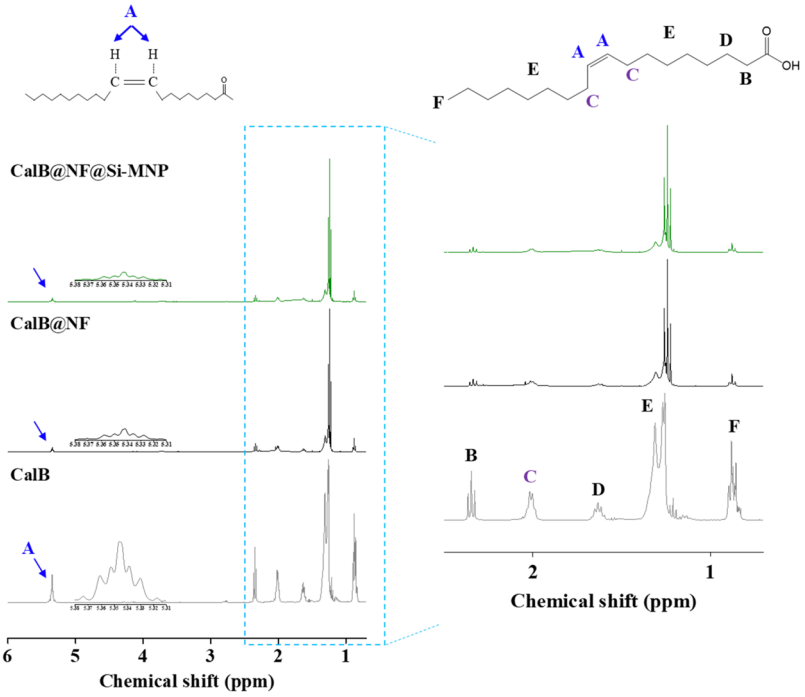

Figure 5. ^{1}H NMR spectra at 45 min of CalB, CalB@NF, and CalB@NF@Si-MNP.

exhibited a release pattern similar to CalB@NF, as CalB@NF is linked to the surface of Si-MNP. The slower release in CalB@NF@Si-MNP is attributed to levan, which, owing to its hydrophilic nature, expands the hydrophilic domain surrounding the enzyme. This expansion increases the effective diffusion range of both CalB and the substrate, thereby diluting their local concentrations and contributing to a relatively slower lipolysis rate. On the other hand, CalB@NF@SiO_2 began releasing oleic acid after 1 h of lipolysis, with a continuous release until 24 h, reaching 100%. The silica coating in CalB@NF@SiO_2 completely encapsulates CalB@NF, making the active site of CalB inaccessible initially, thus delaying the onset of lipolysis by about 1 h. Figure 4c shows the lipolysis rate of CalB, CalB@NF, CalB@NF@Si-MNP, and CalB@NF@SiO_2. The lipolysis rates were 6.55 mmol/h for CalB, 2.49 mmol/h for CalB@NF, 0.92 mmol/h for CalB@NF@Si-MNP, and 0.21 mmol/h for CalB@NF@SiO_2. As seen in Figure 4b, after 2 h of lipolysis, CalB@NF and CalB@NF@Si-MNP completed the reaction at a similar pace. It is important to note that although both levan and silica have abundant −OH groups, the loss of activity in CalB@NF@Si-MNP appears not to be solely a function of these groups. Rather, the immobilization process on the silica surface may impose additional structural constraints or steric hindrance, thereby further reducing the catalytic efficiency of CalB. Furthermore, CalB@NF@SiO_2, in addition to the effects seen in CalB@NF@Si-MNP, also has the active site of CalB masked by the silica, resulting in a 4.5-fold decrease in the lipolysis rate compared to CalB@NF@Si-MNP.

Figure 5 shows the ^{1}H NMR spectra of the enzymatic lipolysis products at 45 min for CalB, CalB@NF, and CalB@NF@Si-MNP. CalB@NF@SiO_2 was excluded from the ^{1}H NMR analysis as no lipolysis occurred at 45 min. A distinct peak for oleic acid, attributed to the double bond, appeared at 5.3 ppm. When this peak was zoomed in, CalB showed the highest intensity, as it had released 100% of the oleic acid at 45 min. Both CalB@NF and CalB@NF@Si-MNP displayed similar intensities, indicating a slower release compared to CalB. Additionally, the ^{1}H NMR analysis at 400 MHz of the oleic acid standard revealed the following peaks: 0.9 ppm (s, $-CH_3$, F), 1.27 ppm (s, $-CH_2$, E), 1.31 ppm (s, $-CH_2$, E), 1.35 ppm (s, $-CH_2$, E), 1.63 ppm (s, $-CH_2$, D), 2.01 ppm (s, $-CH_2$, C), 2.3 ppm (s, $-CH_2$, B), and 5.3 ppm (s, =CH, A). By comparing the ^{1}H NMR spectra of the oleic acid standard with the spectra of CalB, CalB@NF, and CalB@NF@Si-MNP, we observed strong agreement between the standard and the peaks corresponding to the products, confirming the enzymatic release of oleic acid.

Figure 6 shows the reusability of CalB, CalB@NF, CalB@NF@Si-MNP, and CalB@NF@SiO_2 for lipolysis. CalB and CalB@NF cannot be recovered, making it challenging to assess their reusability. However, both CalB@NF@Si-MNP and CalB@NF@SiO_2 demonstrated the ability to be reused multiple times, although their lipolytic activity decreased with each reuse cycle. The initial activities of each immobilized

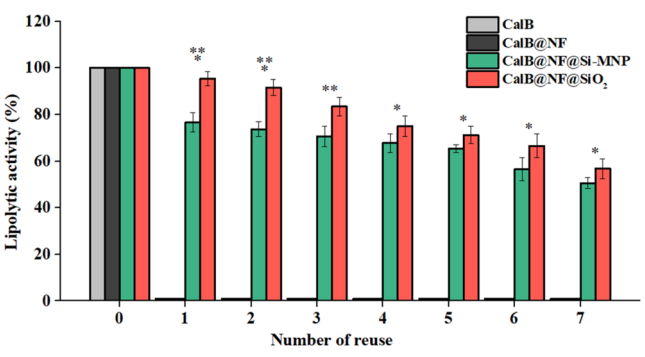

Figure 6. Reusability of CalB, CalB@NF, CalB@NF@Si-MNP, and CalB@NF@SiO_2. Statistical analysis indicates significant differences between CalB@NF@Si-MNP and CalB@NF@SiO_2 for most cycles ($p < 0.05$).

https://doi.org/10.1021/acsomega.4c11216
ACS Omega 2025, 10, 13319−13326

enzyme were measured prior to reuse. Since the Bradford assay results (Figure 3b) indicated differences in the CalB content of each sample, the weights of CalB@NF@Si-MNP and CalB@NF@SiO_2 were adjusted to ensure that each assay contained the same amount of CalB. This normalization allows for a fair comparison of both the initial activity and the subsequent reusability between the two formulations. Overall, CalB@NF@SiO_2 exhibited higher lipolytic activity than CalB@NF@Si-MNP. Specifically, the activity of CalB@NF@Si-MNP dropped sharply to 76% after the first reuse cycle, likely because its structure was more vulnerable to the external environment when bound to the silica surface. In contrast, the silica coating on CalB@NF@SiO_2 provides better protection, resulting in greater stability and enabling a more consistent lipolytic process ($p < 0.05$ reuse cycles).

4. CONCLUSIONS

CalB@NF were successfully encapsulated and immobilized within a silica matrix, resulting in the formation of CalB@NF@SiO_2 and CalB@NF@Si-MNP. Both CalB@NF@SiO_2 and Si-MNP particles exhibited spherical morphologies, with sizes of 304 and 58 nm, respectively. Si-MNP was surface-modified with −Cl silane, followed by the immobilization of CalB@NF. The Bradford assay quantified CalB content, revealing a CalB@NF@Si-MNP to CalB@NF@SiO_2 ratio of approximately 2:1. Enzymatic lipolysis was evaluated by using olive oil, and oleic acid release was measured. The release of oleic acid from CalB@NF@Si-MNP occurred 4.5 times faster than that from CalB@NF@SiO_2. However, CalB@NF@SiO_2 exhibited a more consistent release of oleic acid over 12 times the duration of lipolysis compared to CalB@NF@Si-MNP. Furthermore, CalB@NF@SiO_2 demonstrated superior reusability, which can be attributed to the structural differences between CalB@NF@Si-MNP and CalB@NF@SiO_2. While CalB@NF@Si-MNP exposes the CalB lipase enzyme on its surface, allowing for high catalytic activity and making it ideal for short-term applications, it is more sensitive to external environmental factors. In contrast, CalB@NF@SiO_2 offers enhanced protection to the CalB lipase enzyme, providing a stable environment that is more suitable for long-term use, although with relatively lower catalytic efficiency. These findings suggest that CalB@NF@SiO_2 and CalB@NF@Si-MNP can be effectively utilized, depending on the desired application environment and time, potentially leading to significant cost savings in various industries and enabling their use in continuous processes.

AUTHOR INFORMATION

Corresponding Author

Jeong Ho Chang − *Korea Institute of Ceramic Engineering and Technology, Jinju 52851, Republic of Korea;* orcid.org/0000-0002-8222-4176; Phone: +82 43 913 1510; Email: jhchang@kicet.re.kr; Fax: +82 43 913 1592

Authors

Woo Young Jang − *Korea Institute of Ceramic Engineering and Technology, Jinju 52851, Republic of Korea; Department of Materials Science & Engineering, Yonsei University, Seoul 03722, Republic of Korea*

Yu Jeong Kim − *Korea Institute of Ceramic Engineering and Technology, Jinju 52851, Republic of Korea*

Complete contact information is available at: https://pubs.acs.org/10.1021/acsomega.4c11216

Author Contributions

[‖]W.Y.J. and Y.J.K. contributed equally to this work.

Author Contributions

All authors contributed to the writing of the manuscript. All the authors approved the final version of the manuscript.

Notes

The authors declare no competing financial interest.

ACKNOWLEDGMENTS

This work was supported by the "Cooperative Research Program for Agriculture Science and Technology Development (Project No. PJ01493802)" Rural Development Administration, Republic of Korea.

REFERENCES

(1) Guntermann, A.; Koch, L.; Groger, H. Process Development for the Sustainable and Economic Production of Biobased and Biodegradable High-Performance Lubricants. *ACS Sustainable Chem. Eng.* **2024**, *12* (13), 5086−5091.

(2) Rezaei, S.; Landarani-Isfahani, A.; Moghadam, M.; Tangestaninejad, S.; Mirkhani, V.; Mohammadpoor-Baltork, I. Hierarchical Gold Mesoflowers in Enzyme Engineering: An Environmentally Friendly Strategy for the Enhanced Enzymatic Performance and Biodiesel Production. *ACS Appl. Bio Mater.* **2020**, *3* (12), 8414−8426.

(3) Basso, A.; Serban, S. Industrial applications of immobilized enzymes—A review. *Mol. Catal.* **2019**, *479*, No. 110607.

(4) Khan, N. R.; Rathod, V. K. Enzyme catalyzed synthesis of cosmetic esters and its intensification: A review. *Process Biochem.* **2015**, *50* (11), 1793−1806.

(5) Salihu, A.; Alam, M. Z. Solvent tolerant lipases: a review. *Process Biochem.* **2015**, *50* (1), 86−96.

(6) Navvabi, A.; Razzaghi, M.; Fernandes, P.; Karami, L.; Homaei, A. Novel lipases discovery specifically from marine organisms for industrial production and practical applications. *Process Biochem.* **2018**, *70*, 61−70.

(7) Angajala, G.; Pavan, P.; Subashini, R. Lipases: An overview of its current challenges and prospectives in the revolution of biocatalysis. *Biocatal. Agric. Biotechnol.* **2016**, *7*, 257−270.

(8) Lima, R. N.; dos Anjos, C. S.; Orozco, E. V.; Porto, A. L. Versatility of Candida antarctica lipase in the amide bond formation applied in organic synthesis and biotechnological processes. *Mol. Catal.* **2019**, *466*, 75−105.

(9) Li, N. W.; Zong, M. H.; Wu, H. Highly efficient transformation of waste oil to biodiesel by immobilized lipase from Penicillium expansum. *Process Biochem.* **2009**, *44* (6), 685−688.

(10) Sá, A. G. A.; de Meneses, A. C.; de Araújo, P. H. H.; de Oliveira, D. A review on enzymatic synthesis of aromatic esters used as flavor ingredients for food, cosmetics and pharmaceuticals industries. *Trends Food Sci. Technol.* **2017**, *69*, 95−105.

(11) Schoemaker, H. E.; Mink, D.; Wubbolts, M. G. Dispelling the myths-biocatalysis in industrial synthesis. *Science* **2003**, *299*, 1694−1697.

(12) Soldatkin, O.; Kucherenko, I.; Pyeshkova, V.; Kukla, A.; Jaffrezic-Renault, N.; El'Skaya, A.; Dzyadevych, S.; Soldatkin, A. Novel conductometric biosensor based on three-enzyme system for selective determination of heavy metal ions. *Bioelectrochemistry* **2012**, *83*, 25−30.

(13) Lee, H. R.; Kim, M. I.; Hong, S. E.; Choi, J.; Kim, Y. M.; Yoon, K. R.; Lee, S.; Ha, S. H. Effect of functional group on activity and stability of lipase immobilized on silica-coated magnetite nanoparticles with different functional group. *J. Anal. Sci. Technol.* **2016**, *29* (3), 105−113.

(14) Stauch, B.; Fisher, S. J.; Cianci, M. Open and closed states of Candida antarctica lipase B: Protonation and the mechanism of interfacial activation1. *J. Lipid Res.* **2015**, *56* (12), 2348−2358.

(15) Cho, C. H.; Patel, S.; Rajbhandari, P. Adipose tissue lipid metabolism: lipolysis. *Curr. Opin. Genet. Dev.* **2023**, *83*, No. 102114.
(16) Vaughan, M.; Berger, J. E.; Steinberg, D. Hormone-sensitive lipase and monoglyceride lipase activities in adipose tissue. *J. Biol. Chem.* **1964**, *239* (2), 401−409.
(17) Wu, Q.; Soni, P.; Reetz, M. T. Laboratory evolution of enantiocomplementary Candida antarctica lipase B mutants with broad substrate scope. *J. Am. Chem. Soc.* **2013**, *135* (5), 1872−1881.
(18) Ghanem, A. Trends in lipase-catalyzed asymmetric access to enantiomerically pure/enriched compounds. *Tetrahedron* **2007**, *63* (8), 1721−1754.
(19) Sun, J.; Jiang, Y.; Zhou, L.; Gao, J. Immobilization of Candida antarctica lipase B by adsorption in organic medium. *New Biotechnol.* **2010**, *27* (1), 53−58.
(20) Adlercreutz, P. Immobilisation and application of lipases in organic media. *Chem. Soc. Rev.* **2013**, *42* (15), 6406−6436.
(21) Kirk, O.; Christensen, M. W. Lipases from candida a ntarctica: unique biocatalysts from a unique origin. *Org. Process Res. Dev.* **2002**, *6* (4), 446−451.
(22) Monteiro, R. R. C.; Neto, D. M. A.; Fechine, P. B.; Lopes, A. A.; Gonçalves, L. R.; dos Santos, J. C.; de Souza, M. C.; Fernandez-Lafuente, R. Ethyl butyrate synthesis catalyzed by lipases A and B from Candida antarctica immobilized onto magnetic nanoparticles. Improvement of biocatalysts' performance under ultrasonic irradiation. *Int. J. Mol. Sci.* **2019**, *20* (22), No. 5807.
(23) Mangiagalli, M.; Carvalho, H.; Natalello, A.; Ferrario, V.; Pennati, M. L.; Barbiroli, A.; Lotti, M.; Pleiss, J.; Brocca, S. Diverse effects of aqueous polar co-solvents on Candida antarctica lipase B. *Int. J. Biol. Macromol.* **2020**, *150*, 930−940.
(24) Hundschell, C.; Jakob, F.; Wagemans, A. Molecular weight dependent structure of the exopolysaccharide levan. *Int. J. Biol. Macromol.* **2020**, *161*, 398−405.
(25) Arvidson, S. A.; Rinehart, B. T.; Gadala-Maria, F. Concentration regimes of solutions of levan polysaccharide from Bacillus sp. *Carbohydr. Polym.* **2006**, *65* (2), 144−149.
(26) Sonh, J. H.; Bae, J. H.Levan-Protein Nanocomposite and Uses Thereof. KR Patent KR20210012979A2021.
(27) Rotticci, D.; Rotticci-Mulder, J. C.; Denman, S.; Norin, T.; Hult, K. Improved enantioselectivity of a lipase by rational protein engineering. *ChemBioChem* **2001**, *2* (10), 766−770.
(28) Jang, W. Y.; Sohn, J. H.; Chang, J. H. Thermally Stable and Reusable Silica and Nano-Fructosome Encapsulated CalB Enzyme Particles for Rapid Enzymatic Hydrolysis and Acylation. *Int. J. Mol. Sci.* **2023**, *24* (12), No. 9838.
(29) Song, M.; Chang, J. H. Thermally Stable and Reusable Ceramic Encapsulated and Cross-Linked CalB Enzyme Particles for Rapid Hydrolysis and Esterification. *Int. J. Mol. Sci.* **2022**, *23* (5), No. 2459.
(30) Hartmann, M.; Kostrov, X. Immobilization of enzymes on porous silicas−benefits and challenges. *Chem. Soc. Rev.* **2013**, *42* (15), 6277−6289.
(31) Sun, J.; Zhang, H.; Tian, R.; Ma, D.; Bao, X.; Su, D. S.; Zou, H. Ultrafast enzyme immobilization over large-pore nanoscale mesoporous silica particles. *Chem. Commun.* **2006**, *12*, 1322−1324.
(32) Lee, H. Y.; Jang, W. Y.; Chang, J. H. Reusable and rapid esterolysis of nitrophenyl alkanoates with CalB enzyme-immobilized magnetic nanoparticles. *J. Korean Ceram. Soc.* **2022**, *59*, 527−535.
(33) Tang, W.; Ma, T.; Zhou, L.; Wang, G.; Wang, X.; Ying, H.; Chen, C.; Wang, P. Polyamine-induced tannic acid co-deposition on magnetic nanoparticles for enzyme immobilization and efficient biodiesel production catalysed by an immobilized enzyme under an alternating magnetic field. *Catal. Sci. Technol.* **2019**, *9* (21), 6015−6026.
(34) Lee, S. Y.; Ahn, C. Y.; Lee, J.; Chang, J. H. Amino acid side chain-like surface modification on magnetic nanoparticles for highly efficient separation of mixed proteins. *Talanta* **2012**, *93*, 160−165.
(35) Lee, S. Y.; Lee, J. H.; Chang, J. H.; Lee, J. H. Inorganic nanomaterial-based biocatalysts. *BMB Rep.* **2011**, *44* (2), 77−86.
(36) Tran, D. T.; Chen, C. L.; Chang, J. S. Immobilization of Burkholderia sp. lipase on a ferric silica nanocomposite for biodiesel production. *J. Biotechnol.* **2012**, *158* (3), 112−119.
(37) Mehrasbi, M. R.; Mohammadi, J.; Peyda, M.; Mohammadi, M. Covalent immobilization of Candida antarctica lipase on core-shell magnetic nanoparticles for production of biodiesel from waste cooking oil. *Renewable Energy* **2017**, *101*, 593−602.
(38) Hazarika, K. P.; Borah, J. Study of biopolymer encapsulated Eu doped Fe3O4 nanoparticles for magnetic hyperthermia application. *Sci. Rep.* **2024**, *14* (1), No. 9768.
(39) Gupta, A. K.; Gupta, M. Synthesis and surface engineering of iron oxide nanoparticles for biomedical applications. *Biomaterials* **2005**, *26* (18), 3995−4021.
(40) Křížová, J.; Španová, A.; Rittich, B.; Horák, D. Magnetic hydrophilic methacrylate-based polymer microspheres for genomic DNA isolation. *J. Chromatogr. A* **2005**, *1064* (2), 247−253.
(41) Lee, S. Y.; Lee, S. Y.; Lee, J. H.; Lee, H. S.; Chang, J. H. Biomimetic magnetic nanoparticles for rapid hydrolysis of ester compounds. *Mater. Lett.* **2013**, *110*, 229−232.
(42) Mylkie, K.; Nowak, P.; Rybczynski, P.; Ziegler-Borowska, M. Polymer-Coated Magnetite Nanoparticles for Protein Immobilization. *Materials* **2021**, *14* (2), No. 248.
(43) Kruger, N. J. The Bradford Method For Protein Quantitation. In *Springer Protocols Handbooks*; Springer, 2009; pp 17−24.
(44) Bradford, M. M. A rapid and sensitive method for the quantitation of microgram quantities of protein utilizing the principle of protein-dye binding. *Anal. Biochem.* **1976**, *72* (1−2), 248−254.

https://doi.org/10.1021/acsomega.4c11216
ACS Omega 2025, 10, 13319−13326